Sorting Nanoparticles by Centrifugal Fields in Clean Media

Francesco Bonaccorso,[†,‡] Mirco Zerbetto,[§] Andrea C. Ferrari,[†] and Vincenzo Amendola*[,§]

[†]Cambridge Graphene Centre, University of Cambridge, 9 JJ Thomson Avenue, Cambridge, CB3 0FA, U.K.
[‡]CNR-Istituto Processi Chimico-Fisici, Viale F. Stagno D'Alcontres 37, 98158, Messina, Italy
[§]Department of Chemical Sciences, University of Padova, Via Marzolo 1, I-35131 Padova, Italy

ABSTRACT: The on-demand availability of nanomaterials with selected size and well-defined chemical/physical properties is of fundamental importance for their widespread application. We report two clean, rapid, and non-destructive approaches for nanoparticle (NP) size selection in centrifugal fields. The first exploits rate zonal separation in a high viscosity gradient. The second exploits selective sedimentation of NPs with different sizes. These methods are here applied to metallic nanoparticles (MNPs) with different compositions and surface chemistry, dispersed either in water or organic solvents. The approach is general and can also be exploited for the separation of NPs of any material. We selectively sort both Au and AgNPs with sizes in the 10−30 nm range, achieving chemical-free MNPs with low polydispersivity. We do not use solutes, thus avoiding contamination, and only require low centrifugal fields, easily achievable in benchtop systems.
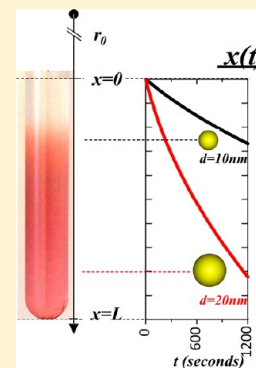
INTRODUCTION

The preparation of nanoparticles (NPs) with well-defined size is of paramount importance for the accurate control of their properties[1−3] and for the investigation of size-dependent chemical and physical phenomena.[4,5]

NPs with well-defined size in the 10−30 nm range are important for several applications, in particular in the field of photonics,[6,7] nanomedicine,[8] and nanobiotechnology.[9] Au and AgNPs of 10−30 nm size offer the best performance for photothermal heating,[10] because the surface plasmon resonance is depressed in NPs smaller than 10 nm,[11,12] due to free electron scattering at surface boundaries,[11,13] while above 30 nm light scattering overwhelms absorption,[11,13] with consequent reduction of light conversion to heat.[10] Plasmon-induced photothermal heating is used for photothermal[14] and photoacustic imaging,[15] as well as for photothermal therapy.[10] Photothermal heating can also be used for plasmon lithography[16] and nanosurgery[17] where 10−30 nm NPs offer the best compromise between efficient heating and resolution.[10] The NPs chemical[18,19] and catalytic[19−21] properties are significantly influenced by their size. As an example, the surface area per unit mass of 10 nm NPs is 5 times that of 50 nm ones; thus, 10 nm NPs have higher catalytic activity with respect to 50 nm ones.[22] The catalytic rate constant, i.e., the combined reactivity of all surface catalytic sites,[20,21] increases ∼32% for 13 nm AuNPs compared to 6 nm ones.[21] The magnetic properties are also size dependent,[23,24] and, e.g., the superparamagnetic iron oxide NPs with the largest magnetic moment are those in the 10−25 nm range,[23,24] because the transition from ferromagnetic to superparamagnetic behavior in iron oxide NPs is observed at 25 nm,[23,25] and the magnetic moment of NPs scales with their volume.[23] In nanomedicine, 10−30 nm NPs offer excellent performances for in vivo selective accumulation in targeted tissues[8,26−28] and reduced clearance rates.[8,26−28] This is because NPs below 10 nm are cleared by kidneys less than 24 h after injection,[29] which reduces the time available for reaching the target with consequent low accumulation yields[29] and the need for repeated NP injections.[29] NPs larger than 30 nm are efficiently sequestered by macrophages of the reticuloendothelial system[28] and Kupffer cells[30] in the liver, with a consequent accumulation in undesired sites[26−28] and clearance by multiple pathways on the time scale of weeks to years.[26−28] 10 nm NPs undergo a 2-fold increase in circulating time than larger NPs (e.g., 50-100 nm) due to a slower sequestration by the reticuloendothelial systems.[28] E.g., ref 31 demonstrated that 10 nm AuNPs were present in various organ systems including blood, liver, spleen, kidney, testis, thymus, heart, lung, and brain, whereas larger NPs (50-100 nm) were only detected in blood, liver, and spleen. NPs uptake and removal is also size dependent:[31−34] uptake of 14 nm AuNPs is 33% higher than 74 nm AuNPs.[34] Smaller AuNPs exocytose[35] at a faster rate than larger ones.[33,34] E.g., the exocytosis of 14 nm AuNPs is two times higher than 74 nm AuNPs and five times higher than 100 nm AuNPs.[33] Purity, i.e., the absence of toxic chemicals, is also a crucial point for bioapplications.[36]

Metallic NPs (MNPs) are at the center of a rapidly expanding research area, with applications ranging from photovoltaics,[37,38] to optical emitters,[39] waveguides,[40] surface-enhanced Raman scattering (SERS),[41−43] SERS-based sensors,[44,45] and nanoantennas,[46] just to cite a few. The optical properties of MNPs are dependent on their size[6,7,47] and only NPs with clean surface are effectively coupled with other

materials, like graphene,[38] Raman active molecules,[6] and semiconductors.[48]

Here we report two methodological advances to sort (i.e. separate in a range of sizes) MNPs with no need of solutes or additives. In the first, we use rate zonal separation (RZS) in a viscosity gradient (VG) obtained by mixing common solvents, such as water or ethanol (EtOH), with pure liquids with high viscosity, such as ethylene glycol (EG) or glycerol. In the second, we use sedimentation-based separation (SBS), without any density gradient medium (DGM) or additional solute, by selecting the appropriate range of relative centrifugal forces, to achieve selective (i.e., in a dimension range) and sequential (i.e., exploiting successive centrifugation runs) sedimentation of the largest particles in solution. Both our approaches are applied to 10−30 nm MNPs, where most previous attempts failed[49−51] or required additional (unwanted) solutes.[52−56] We test our methods on MNPs with different composition, surface stabilization, and coating, including AuNPs and AgNPs obtained by laser ablation in pure water. These are ideal candidates for post-synthesis sorting because of their chemical purity,[47] absence of stabilizers,[47] and a standard deviation (SD) of the average NP size ~ 60%.[47] The separation strategies reported in this article have general validity and can be applied to NPs of any other material.

■ BACKGROUND

In wet chemistry synthesis, such as synthesis in liquid solution of NPs from soluble precursors,[4] monodispersed NPs are obtained by the use of coating/stabilizing agents.[4,19,57−61] Monodispersed MNPs are obtained by using thiolated ligands[5,19] or citrate molecules.[4,5,19,62] A post-synthesis size selection procedure[49,52,53,55,63−69] can be a viable alternative to the use of coating/stabilizing agents, especially when these must be avoided because they are toxic[36] or hamper further functionalization with desired molecules.[70] Several approaches have been suggested for post-synthesis size selection, such as preparative centrifugation,[64,67,68,71] density gradient ultracentrifugation (DGU),[49,52,53,55,63,69] size exclusion chromatography,[68] membrane filtration,[65] selective precipitation,[72] or electrophoresis.[66] Other post-synthesis treatments, such as laser irradiation,[25,73,74] can also be used for size refinement, i.e., to reduce the NP size polydispersivity.

The application of centrifugal fields to nanomaterials in solution is called differential ultracentrifugation.[75] When the nanomaterials are dispersed in a uniform gradient medium, this process is referred to as SBS,[75] while it is called DGU when performed in a DGM.[76,77] Both SBS and DGU can spatially separate particles based on their size.[75−77] SBS separates nanomaterials exploiting their sedimentation coefficient,[75] commonly reported in Svedberg (S) units, where 1 S corresponds to 10^{-13} s.[75] The sedimentation coefficient determines the time needed for the NPs to sediment out of the fluid in which they are dispersed, under the centrifugal force acting on them.

In DGU, particles are ultracentrifuged in a preformed DGM.[76−78] During the process, they move along a cuvette until they reach the corresponding isopycnic point, i.e., the point where their buoyant density equals that of the surrounding DGM.[78] The buoyant density is defined as the density of the medium at the corresponding isopycnic point (measured in g/cm³). The buoyant density depends on the dispersion,[79] on the type of surfactant,[80] and may also change with gradient medium[79] or, for the same DGM, according to

the pH.[79] Such process depends only on the buoyant density of the particles and is also known as isopycnic separation.[78] In RZS, the ultracentrifugation is stopped during the transient centrifugal regime, before the particles arrive at their isopycnic points.[81] RZS exploits differences in the sedimentation coefficient.[81] Thus, objects with different S values will travel along the cuvette at different sedimentation velocities.[78,81] This will cause a spatial separation.[81]

DGU was originally developed for the separation of biological particles, such as cells,[82,83] viruses,[81,84] deoxyribonucleic acid (DNA),[85] etc. This technique is now commonly used to sort nanomaterials. Isopycnic separation was used to sort nanotubes by diameter,[86] metallic vs semiconducting nature,[87] chirality,[80] handedness,[88,89] and graphite flakes by number of layers.[90] RZS was used to separate nanotubes by length,[91] graphene oxide sheets by size[92] and surface chemistry,[92] several types of small sized (i.e., < 10 nm) ligands stabilized inorganic NPs, such as semiconductor quantum dots,[49,63,93,94] thiolated metal clusters,[3] thiolated AgNPs,[49] to separate Au nanospheres from nanorods,[51] Au nanowires,[49] nanoplates,[50] and small aggregates of polymer encapsulated AuNPs.[52,53] RZS is a quick (~10−20 min)[55,81,92] and scalable process (ultracentrifuges can process liters of dispersions per run), thus avoiding drawbacks of other techniques, such as the limited scalability of size exclusion chromatography,[68] the very long processing time of selective precipitation[72] or electrophoresis,[66] the agglomeration frequently observed with membrane filtration,[65] size exclusion chromatography[68] and electrophoresis,[66] and the imprecise sorting, i.e., SD of the order of 100% of the average size of sorted NPs, typical of electrophoresis[66] and size exclusion chromatography.[68] Moreover, separation strategies such as membrane filtration[65] will cause aggregation of NPs due to removal of stabilizing agents. E.g., citrate stabilized AuNPs,[54] cetyltrimethylammonium bromide stabilized Au nanorods,[54,56] or surfactants stabilized nanotubes[80] undergo irreversible aggregation upon removal of the stabilizing agents, a process carried out via dialysis.[80]

The liquid solutions commonly used for DGU have a maximum density of 1.4 g/cm³.[49,80] Higher density media, such as bromoform,[95] borotungstate of cadmium,[96] etc., are toxic.[97] Although non-toxic alternatives exist, such as sodium polytungstate,[98] the maximum density achievable is 3.1 g/cm³.[99] Therefore, isopycnic separation in a density gradient is not possible for NPs with densities over 3.1 g/cm³, a value much lower than the density of most inorganic materials, such as metals (i.e., Au 19.1 g/cm³),[100] metal oxides (i.e., Fe_3O_4 5.2 g/cm³),[100] or semiconductors (cadmium sulphide 4.82 g/cm³).[100] Furthermore, the most common density gradients are prepared by adding DGMs in the form of solutes, such as CsCl,[79,101] sucrose,[102,103] or iodixanol.[80,82,83,86] This affects the dispersion purity, and these solutes are difficult to remove after the separation process. RZS is thus the alternative for high density particles. Density gradients produced using salts[79,101] are less stable with respect to those produced with sucrose[102,103] and Optiprep,[80,82,83,86] due to their low viscosity;[104] therefore, these are not ideal for RZS. Sorting by transient motion causes a faster sedimentation for higher-mass particles compared to lower-mass ones.[55] This can be mitigated by using high-viscosity DGMs, thus slowing the sedimentation of high-mass particles to the point where structurally distinct fractions (f) can be collected following centrifugation.[55] Sucrose has high viscosity,[105] exponentially increasing at high concentrations.[105] It is thus very popular for RZS.[103] Optiprep

has also high viscosity,[82,83] but this is almost constant as a function of the gradient density.[106] It was recently used for RZS of silica-coated AuNPs,[55] while ref 54 created a high-viscosity density gradient by dissolving polyvinylalcohol (PVA) in an aqueous solution. This allowed the separation of NPs with size in the 30−200 nm range, otherwise not possible by isopycnic separation in a density gradient.[54,55]

The DGM can also interfere with the stability of the nanomaterial dispersions[107,108] because salts present in DGMs reduce the electrostatic stability of charged NPs dispersed in liquid solutions,[109] and NPs can undergo aggregation during preparative ultracentrifugation.[103] The DGM can adsorb on the NP surface.[103] Salts can induce strong aggregation on hydrophobic solutes[107,108] that may affect the separation process itself. A similar effect can happen when sucrose is used.[103] Moreover, DGMs containing CsCl cannot be used to sort citrate stabilized NPs because saline solutions induce aggregation of citrate coated/unstabilized NPs.[110−112]

The high weight fraction of polymers can also interfere with NP stability,[54] requiring the further addition of toxic stabilizers,[113] such as cetyl trimethyl ammonium bromide (CTAB).[54] PVA can also adsorb on the NP surface.[19,114] The PVA molar mass (10 000−40 000 Da)[115] also complicates the purification of NPs in the 10−30 nm range by dialysis[65] or size exclusion chromatography[68] because the size of the unwanted polymer chains is comparable to that of the NPs.[54] In addition, the high weight fraction needed for the experiments reported in ref 54 would require multiple centrifugation runs for each fraction, in order to remove the unwanted PVA by sedimentation and redispersion. Other media, such as mixtures of cyclohexane, C_6H_{12}, and tetrachloromethane, CCl_4, have also been proposed for the separation of AuNPs.[49] However, both solvents have health and environmental issues.[116] In particular, CCl_4 causes liver, kidney, and central nervous system damage.[116]

For these reasons, here we use two clean, rapid, and non-destructive approaches for NP size selection, based either on RZS and SBS, without the use of solutes, thus avoiding surface contamination.

■ EXPERIMENTAL DETAILS

Materials. AuNPs and AgNPs are obtained by laser ablation synthesis in solution (LASiS), as for refs 47, 117. Light pulses of 9 ns at 1064 nm from a Nd:YAG Quantel YG981E laser are focused with a 10 cm focus lens on a 99.99% pure metal plate placed at the bottom of a cell containing a 10^{-5} M NaCl solution in bidistilled water, with a fluence of 10 J cm^{-2} and 10 Hz repetition rate, for 60 min. PEG coated AuNPs in water are obtained by adding 1 mM aqueous solution of thiolated PEG (MW 5000, from Lysan Bio) to LASiS-AuNPs. Excess PEG is removed by dialysis. The PEG coated AuNPs are then transferred in EtOH by drying the aqueous solution and re-dispersing the product in EtOH. Citrate stabilized 10 nm AuNPs in water are sourced from Sigma Aldrich.

Rate Zonal Separation in Viscosity Gradient. The gradient (in viscosity and density) is formed directly in a cuvette (Seton, ultra clear open-top, 14 × 89 mm, capacity 13.2 mL) by stacking different layers (1 mL each) prepared by mixing water (0.9×10^{-3} kg m^{-1} s^{-1} at 25 °C equivalent to 0.9 mPa·s) with a high viscosity liquid, such as EG (16.1 mPa.s), with proportions of EG/H$_2$O varying linearly from 1:0 to 0.2:0.8 from the bottom to the top in 9 successive steps. This creates a step gradient. At the top, we add the LASiS-MNPs

(AuNPs or AgNPs). The cuvette is capped and left in vertical position in order to stabilize the gradient for 1 h prior to VG-RZS.

VG-RZS is carried out via preparative ultracentrifugation (Sorvall WX ultra100 ultracentrifuge) in a TH641 swinging bucket rotor at 20 kRPM for 20 min at 15 °C. The average and maximum accelerations are ∼49 360g and ∼68 600g, respectively, where g is the gravitational acceleration. After VG-RZS, the sorted MNPs are extracted following the fractionation procedure described in refs 80, 87, and 118 for the extraction of single-wall carbon nanotubes. We use upward displacement fractionation[81] exploiting a syringe pump. Fluorinert FC-40 ($\rho \approx 1.85$ g/cm^3; Sigma-Aldrich) is inserted with a needle at the bottom pushing the gradient up into an inverted collection needle. The distance between the top of the dispersion and the upper enriched band is measured using a slide caliper, and the corresponding volume calculated. This is then extracted and discarded by injecting the same volume of Fluorinert at the bottom of the cuvette. Once the bands of interest are at the top, ∼600 μL Fluorinert is injected to extract the same volume of dispersion containing the separated MNPs. In our case, ∼600 μL correspond to a length of ∼8 mm along the cuvette. The same separation and fractionation procedures are carried out for citrate stabilized commercially available AuNPs sorted in a water/EG gradient without any additional stabilizer, to show that our separation technique is suitable also for AuNPs with a different type of surface stabilization with respect to LASiS-AuNPs.

We also test our separation procedure with different aqueous mixtures, such as water/polyethylene glycol 200 (PEG-200) and water/glycerol. In the first case, we use water/PEG-200 mixtures from 0.5:0.5 to 0.9:0.1, by stacking 10 layers (1 mL each) of decreasing PEG-200 concentration from the bottom to the top. This separation is carried out with a Sorvall WX ultra100 ultracentrifuge in a TH641 swinging bucket rotor at 20 kRPM for 20 min. In the second case, we use water/glycerol mixtures from 0.7:0.3 to 0.95:0.05, by stacking 6 layers (1 mL each) of decreasing glycerol concentration from the bottom to the top. This separation is carried out in a benchtop Thermo Scientific centrifuge IEC CL10, equipped with a swinging rotor model O-G26 and VWR cuvettes (borosilicate glass with round-bottom, open-top, 13 × 100 mm, capacity 8 mL) at low relative centrifugal force (rcf) of 2500 for 120 mins. The rcf is a dimensionless quantity that refers to the force applied to a certain mass, relative to that experienced by the same mass when subjected to the gravitational acceleration. Thus rcf = 2500 means that the particles are subjected to an acceleration of 2500 g. In both cases, the fractionation is carried out following the aforementioned procedure.

We also separate PEG-coated AuNPs dispersed in ethanol, using EtOH/EG mixtures from 0.5:0.5 to 0.9:0.1, by stacking 5 layers (1 mL each) of decreasing EG concentration from the bottom to the top. This is carried out in a benchtop centrifuge (Thermo Scientific IEC CL10 equipped with a swinging rotor O-G26) and VWR cuvettes at low rcf (2500). This centrifuge requires a smoother gradient and longer centrifugation time (75 min), due to the lower rcf with respect to the Sorvall WX ultra 100. The fractionation procedure is carried out as described above.

Sedimentation-Based Separation. SBS is carried out with 1.5 mL plastic Eppendorf cuvettes in a benchtop Eppendorf centrifuge 5430, equipped with a fixed angle rotor, FA-45-24-11-HS. The cuvettes are filled with 1 mL LASiS-

AuNPs and then centrifuged for 1 h in the 50−750 rcf range with intervals of 50 rcf. After each run, the supernatant is collected and either centrifuged at higher speed or stored for analysis, while the lower fraction (∼100 μL of concentrated dispersion at the bottom of the cuvette) is collected for spectroscopic characterization at each centrifugation step. The supernatant and 100 μL concentrated dispersion are sequentially extracted with a micropipette. The same procedure is followed for the centrifugation of AuNPs in a wider range of rcfs: 50−5000 (30 min for each run) and 50−11000 (15 min for each run).

We apply selective SBS also to LASiS-AgNPs. The dispersions are centrifuged for 1 h in the 50−750 rcf range, with intervals of 50 rcf. For the subsequent centrifugations and extraction we follow the same procedure as for AuNPs.

Characterization. The attenuation of light through a sample of MNPs is due to a combination of absorption and scattering.[11] We use a Varian Cary 5 spectrometer to measure the optical extinction spectra, i.e., the sum of absorption and scattering.[11] A JEOL JEM 3010 operating at 300 kV and equipped with a Gatan Multiscan CCD Camera model 794 is used for transmission electron microscopy (TEM). The samples for TEM are prepared by evaporating MNP dispersions on a copper grid coated with an amorphous carbon holey film. More than 300 NPs for each sample are analyzed for the calculation of average size and SD. Optical extinction spectra of AuNPs are compared with those calculated with the Mie model,[11,119] using the optical constants of Au from ref 120, corrected for size according to refs 5, 11. The full width at half-maximum (FWHM) of the extinction spectra is calculated with Lorentzian fits.

■ RESULTS

Figure 1a shows the cuvette before preparative ultracentrifugation, while Figure 1b shows it after VG-RZS at 20 kRPM for 20 min. During the process, MNPs move along the cuvette, dragged by the centrifugal force. The optical extinction spectra of dispersions containing 5−60 nm AuNPs have a band centered at ∼520 nm.[11,19] This is due to extinction of incident light[11] and it is originated by the excitation of the surface plasmons in AuNPs.[11,47] Therefore, only red light is transmitted through these AuNPs dispersions, while the electromagnetic spectrum with wavelength equal or shorter than 520 nm is absorbed and scattered by the AuNPs.[11,19] The appearance of the red color along the cuvette indicates that AuNPs move from top to bottom, due to the centrifugal force.

In the 10−30 nm range, the FWHM of the surface plasmon extinction depends on the reciprocal of AuNPs size d, i.e., FWHM $\propto d^{-1}$.[5,11,121−124] This is called intrinsic size effect,[11−13,121] and it is due to electron scattering at particle surfaces,[11] which gains importance for decreasing d.[5,11] Measuring the surface plasmon resonance (SPR) FWHM is the best way to get information on the AuNP size by their extinction spectra,[5,11] and this method is more reliable than the red shift of the SPR for AuNPs of 10−30 nm.[5] In order to provide a clear visualization of the trend of the FWHM in the different fractions, the experimental extinction spectra in Figure 1c are normalized as 1 at 450 nm, where Au interband transitions dominate the extinction properties of AuNPs,[5,11] in order to compare the FWHM of the surface plasmon band of each fraction. Figure 1c shows that a higher intensity of the surface plasmon peak in the normalized spectrum corresponds to a lower FWHM[5,11,13,121−124] and, consequently, to larger
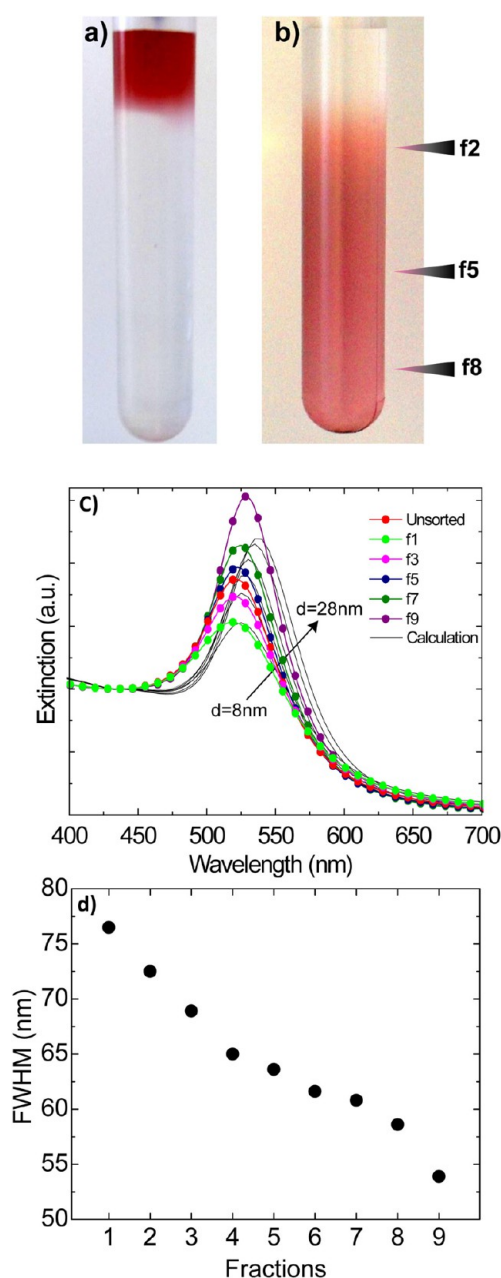
Figure 1. Cuvette filled with AuNPs (a) before and (b) after VG-RZS. (c) Theoretical and experimental extinction spectra of AuNPs. Dotted lines are fractions collected at different positions along the cuvette. All spectra are normalized at 450 nm. Solid lines are Mie model calculations of the extinction spectra of AuNPs with size from 8 to 28 nm. The trend of calculated spectra (indicated by the arrow) agrees with the experimental one, thus confirming that the AuNP size increases moving from the top to the bottom of the cuvette. (d) AuNPs SPR band FWHMs for fractions extracted along the cuvette.

d.[5,11,13,121−124] The normalized extinction spectra show that the AuNPs SPR intensity increases moving from the top (low viscosity and density) to the bottom (high viscosity and density) of the cuvette. It means that larger NPs are found at the bottom of the cuvette. Figure 1d shows that the FWHM of the SPR band of AuNPs decreases along the cuvette.

Figure 1c compares the experimental data with calculations performed exploiting the Mie model[5,11,125] for NPs with increasing size from 8 to 28 nm. This is based on the resolution of the Maxwell equations in spherical coordinates using a
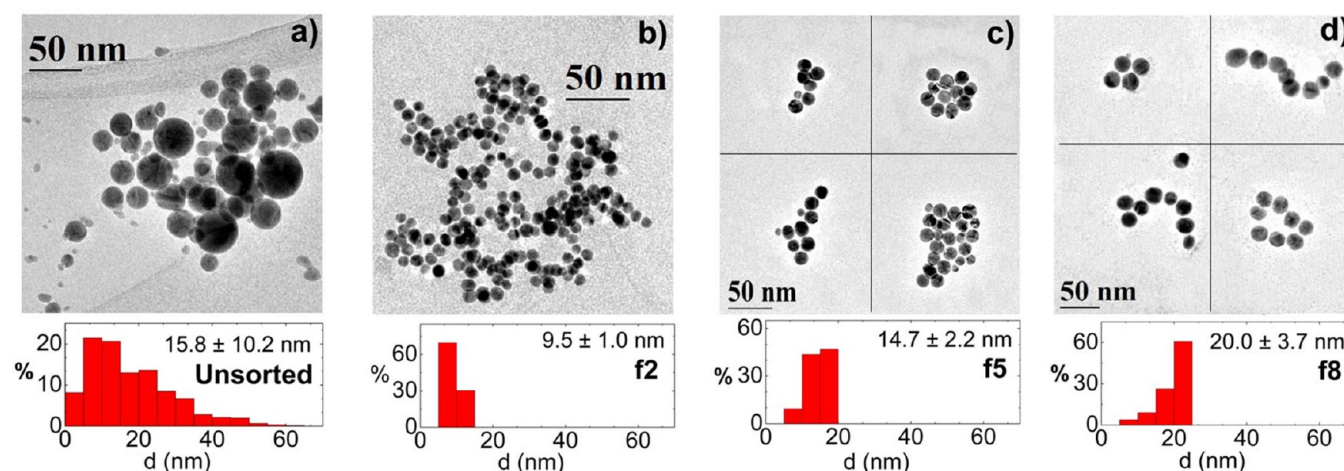
Figure 2. Representative TEM images and size distribution of AuNPs (a) before and (b−d) after RZS: (b) f2, (c) f5, and (d) f8.

multipole expansion of electric and magnetic fields, and accounting for the discontinuity of the dielectric constant between the sphere and surrounding medium.[11,126] Extinction spectra are calculated considering a single spherical NP having the dielectric properties of Au and size variable between 8 and 28 nm. These calculations show a general agreement with experiments, thus confirming that the AuNPs size increases moving from the top to the bottom of the cuvette. As shown in Figure 1d, the FWHM goes from 53 nm for fraction 1 to 77 nm for fraction 9 (i.e., a difference of 24 nm), while the maximum of the SPR red shifts only 9 nm going from f1 to f9 (Figure 1c).

TEM analysis corroborates the conclusions derived from the analysis of the extinction spectra, further confirming that VG-RZS sorts the initially polydispersed AuNPs (size from 0 to 50 nm and SD ~65% of the average size; see Figure 2a) in fractions with lateral sizes increasing from 10 nm (f2) (Figure 2b), ~ 15 nm (f5) (Figure 2c), to 20 nm (f8) (Figure 2d), with SD between 11% and 18% of the average size (see Table1).

Table 1. Average Size and SD of Pristine and Sorted Au and AgNPs, As Measured by TEM

MNPs	sample	size (nm)	SD (nm)	SD (%)
Au	unsorted	15.8	10.2	65
		9.5	1.0	11
Au	VG-RZS	14.7	2.2	15
		20.0	3.7	18
		7.8	1.7	22
Au	selective SBS	19.1	4.2	22
		26.7	8.1	30
Ag	unsorted	23.3	8.2	35
Ag	VG-RZS	22.0	3.4	15
		31.1	5.0	16
Ag	selective SBS	16.0	2.8	17
		34.7	8.0	23

Therefore, the polydispersivity of AuNPs size for the extracted fractions is reduced with respect to unsorted LASiS-AuNPs. We also note that AuNPs do not undergo aggregation or coagulation in the H_2O/EG mixtures, although they are not stabilized by any type of ligand or other molecules.[47] In order to prove the surface accessibility of AuNPs sorted by our VG-RZS procedure in water/EG we add thiolated PEG to fraction f7 and then test the stability against acidic pH. As shown in

Figure 3, no aggregation of AuNPs is observed at pH 1, because the SH group can bind to the AuNPs surface.[19] On the
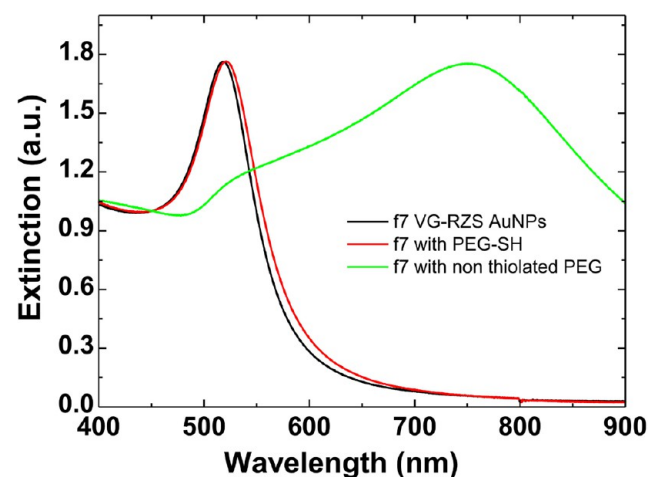
Figure 3. Black line: extinction spectrum of fraction f7 for the VG-RZS AuNPs of Figure 1c. Red line: extinction spectrum of fraction f7 after addition of PEG-SH (MW 5000), at a final concentration of 10^{-5} M, for pH = 1. Green line: extinction spectrum of fraction f7 after addition of non-thiolated PEG (MW 5000), at a final concentration of 10^{-5} M, for pH = 1.

contrary, aggregated AuNPs undergo modifications of extinction properties due to plasmon hybridization,[5,129] which appears as a SPR broadening and red shift.[129] This is what we observe by adding non-thiolated PEG with the same MW (5000 Da) and concentration (10^{-5} M), since no stabilization against acidic pH is seeen (green line in Figure 3a).[5,47,129]

Consequently, VG-RZS in a high viscosity medium overcomes a major problem of AuNPs produced by LASiS, i.e., their polydispersivity,[47] while retaining the uncoated surface[47] and the high purity of the colloidal suspension,[47] typical of LASiS-AuNPs.

We then use this approach on MNPs with a different surface coating: citrate stabilized AuNPs and AuNPs coated with thiolated PEG. In particular, we sort commercially available, citrate AuNPs, stabilized in a water/EG gradient, without any additional stabilizer and without observing aggregation, contrary to what was previously reported for water/PVA gradients[54] (see Figure 4). Indeed, in ref 54, the addition of a

toxic solute, such as cetyl trimethyl ammonium bromide (CTAB), was needed to avoid coagulation.
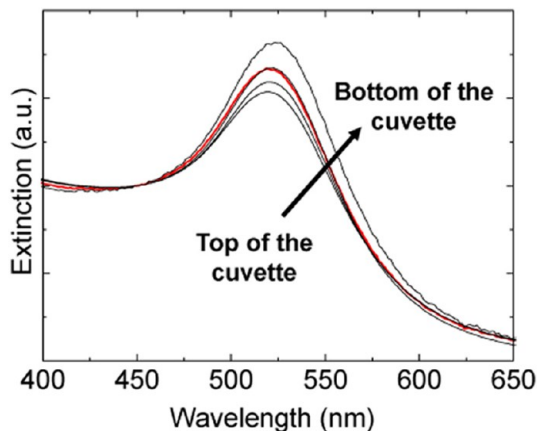
Figure 4. Extinction spectra of fractions of citrate stabilized commercial AuNPs sorted in a water/EG gradient, collected at different positions along the cuvette. The extinction spectrum of the unsorted AuNPs is reported in red. All spectra are normalized at 450 nm.

By the same VG-RZS procedure, MNPs with different composition such as LASiS-AgNPs can also be sorted, as shown in Figure 5. The appearance of the yellow color along the cuvette indicates that AgNPs move from top to bottom, due to the centrifugal force. The yellow color is due to the excitation of surface plasmons in AgNPs, since only yellow light is transmitted through these dispersions.[11]

Preparing gradients by mixing standard solvents, such as ethanol, with high viscosity solvents (i.e., EG, glycerol, etc.) is a simple procedure that can also be applied to MNPs dispersed in organic solvents, e.g., Figure 6a shows that, due to the applied centrifugal force, PEG-coated AuNPs dispersed in ethanol move from the top to the bottom of the cuvette. The normalized extinction spectra show that the PEG-coated AuNPs SPR band increases moving from the top to the bottom of the cuvette (see Figure 6b). The FWHM of the SPR bands decreases along the cuvette from f1 to f4 (see Figure 6c), consistent with the concomitant increase of AuNPs size.

We perform VG-RZS also using other low-cost pure solvents, such as PEG-200 (viscosity, η, ~60 mPa·s; density, ρ, 1.12 g/

cm³)[127] or glycerol ($\eta \approx 1.5 \times 10^3$ mPa·s; $\rho = 1.26$ g/cm³),[128] with viscosity higher than EG, and miscible both with water[128] and many other organic solvents.[128] In particular, gradients with the same viscosity of a water/EG mixture can be obtained by adding a reduced amount of PEG-200 (see Figure 7a) or glycerol (see Figure 7b).

Although VG-RZS carried out in high viscosity pure media is a clean, versatile, and rapid sorting methodology, the size selection of MNPs directly in the original dispersion without adding other solvents would be ideal, being simpler and faster even with respect to VG-RZS, both for sorting and for post-processing treatments.

Therefore, we develop a second approach to sort MNPs via selective SBS using a benchtop preparative centrifuge. Figure 8a shows the AuNPs in the cuvette before selective SBS. As indicated in Figure 8b,c, after centrifugation for 1 h in the 50−200 and 250−750 rcf ranges the dispersions are red. Aggregated AuNPs undergo modifications of extinction properties due to plasmon hybridization,[5,129] which appears as a shift from red to violet/blue, while the extinction spectrum shows SPR broadening and red shift.[129] Since the AuNP colloid is red, this indicates that no aggregation takes place because the applied centrifugal force (in the range 50−750 rcf) is lower than the repulsion force among LASiS-AuNPs. Indeed, centrifugal fields lower than in ordinary DGU[54,55] are used throughout the experiment. Extinction spectra in Figure 8d confirm no aggregation in the AuNPs at the bottom of the cuvette, since no SPR modifications are detected, i.e., the SPR is neither red-shifted nor broadened compared to the initial AuNP dispersion.

Large AuNPs sediment at the bottom of the cuvette. The FWHM of the plasmon band of the fractions extracted after each selective SBS run increases with centrifugal field. Because of the proportionality of FWHM to the reciprocal of the AuNPs size,[5,11] this is consistent with larger particles selectively and sequentially sedimenting with increasing rcf. TEM further confirms the selectivity. Indeed, the MNP sizes of the starting dispersion are in the range 0−60 nm, with average 15.8 nm and SD 65% of the average size (see Figure 9a). After the first selective SBS in the 50−200 rcf range, the sediment shows MNPs with size in the range 5−55 nm, average 26.7 nm, and SD ≈ 30% (Figure 9b). After the second selective SBS, in the 200−750 rcf range, TEM in Figure 9c shows that the sediment has size in the range 5−30 nm, average value 19.1 nm, and SD ≈ 22%, while the MNPs in the supernatant have a size
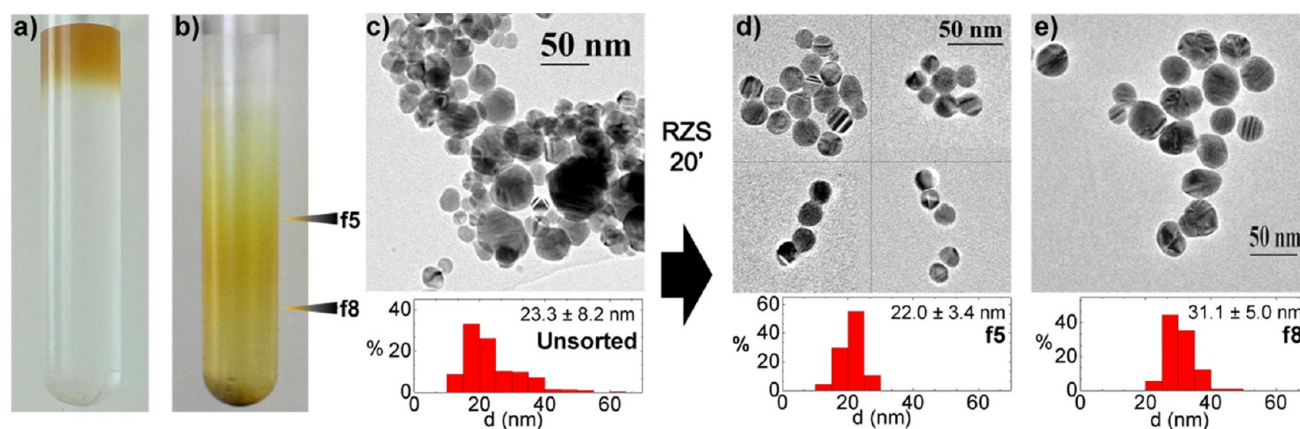
Figure 5. Cuvette filled with (a) unsorted AgNPs and (b) after VG-RZS. Representative TEM images and size distribution of (c) unsorted AgNPs and (d,e) after VG-RZS, extracted at different levels: (d) f5 and (e) f8.
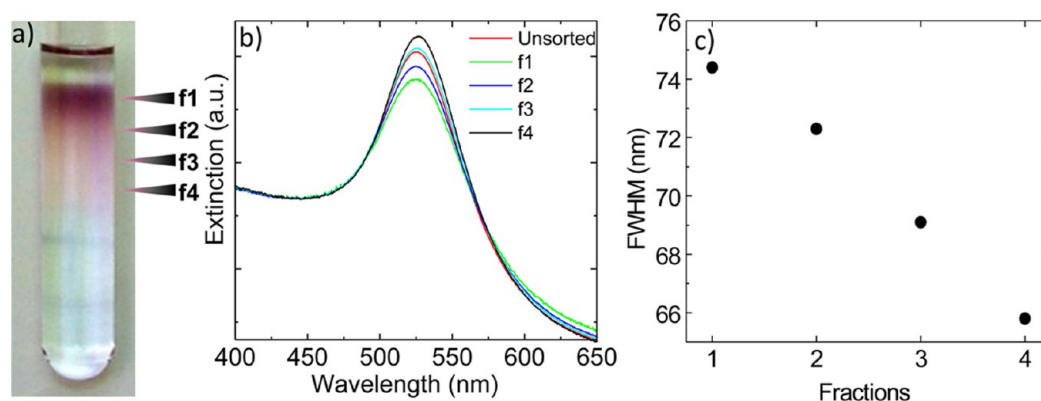
Figure 6. (a) Cuvette after VG-RZS of PEG-coated AuNPs dispersed in EtOH. (b) Extinction spectra of unsorted PEG-coated AuNPs dispersed in EtOH belonging to different fractions. The width of the plasmon band decreases for fractions extracted at increasing distance from the top of the cuvette, f1 to f4. All spectra are normalized at 450 nm for comparison. (c) SPR band FWHM for AuNP fractions along the cuvette.
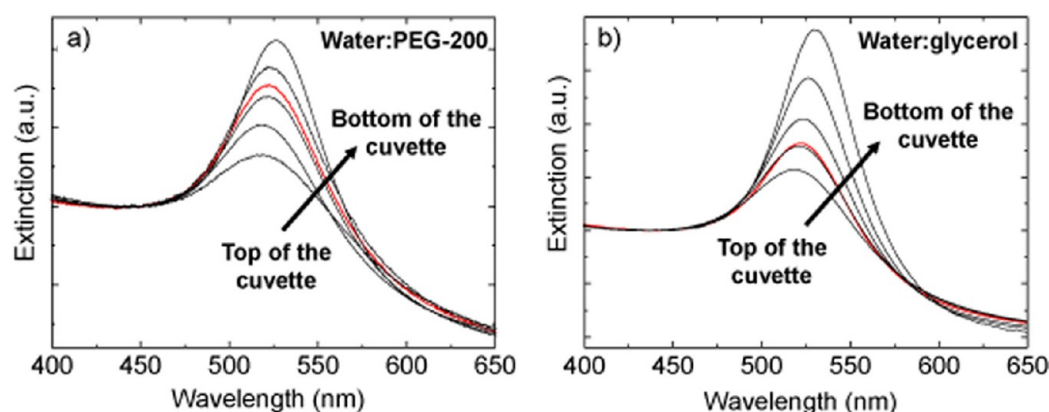
Figure 7. AuNPs sorted in (a) water/PEG-200 and (b) water/glycerol gradients. Extinction spectra of fractions collected at different positions along the cuvette. The extinction spectra of unsorted AuNPs are in red. All spectra are normalized at 450 nm.
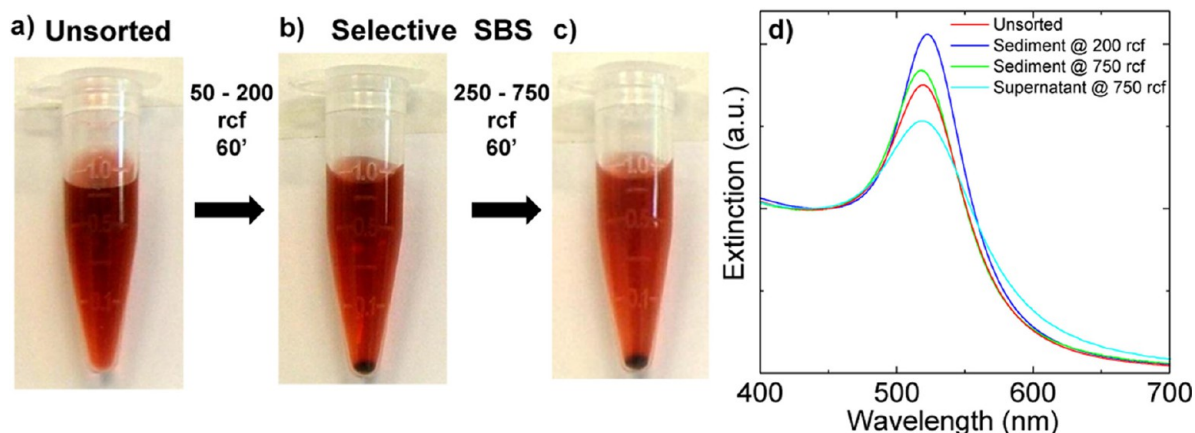
Figure 8. Selective SBS of AuNPs: cuvette (a) before and (b,c) after centrifugation, in the (b) 50−200 rcf and (c) 250−750 rcf ranges. (d) Extinction spectra of the unsorted AuNPs dispersion, the sediment after the two selective SBS runs, and the supernatant of the dispersion centrifuged at 750 rcf. All spectra are normalized at 450 nm.

reduction with respect to the starting material. The extracted MNPs have sizes in the 0−15 nm range, average value 7.8 nm, and SD ≈ 21%, (see Figure 9d). Our results show that the best sorting (i.e., narrowest size distribution) is obtained for the smallest NPs (see Table 1). Indeed, the latter have a smaller sedimentation coefficient with respect to the larger ones and are thus retained in dispersion during centrifugation. This is in agreement with results obtained for two-dimensional materials,

such as graphene flakes, where high concentration of single layers (>60%)[130,131] was achieved with flakes having small lateral size (~20 nm average).[131]

Since no other chemical compounds are added during SBS, NPs maintain the original surface accessibility of LASiS-NPs, discussed in ref 47. Hence, MNPs sorted by SBS retain all the advantages of MNPs produced by LASiS in ultraclean liquids,[47] i.e., uncoated surface[47] and high purity.[47] The rcf and the
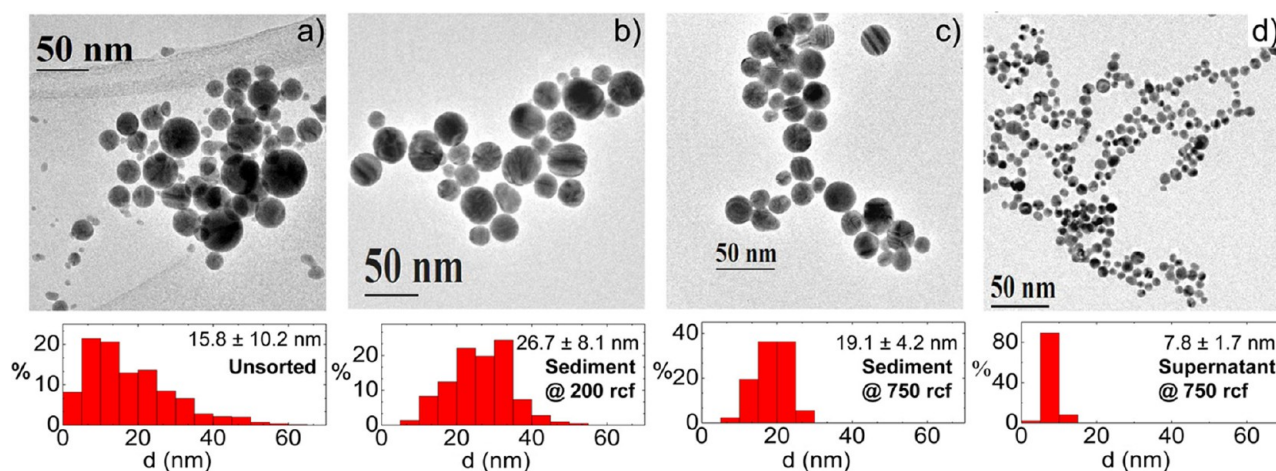
Figure 9. Representative TEM images and size distributions of AuNPs for (a) the unsorted AuNPs, after selective SBS of the sediment at (b) 200 and (c) 750 rcf, and (d) the supernatant extracted after SBS at 750 rcf.
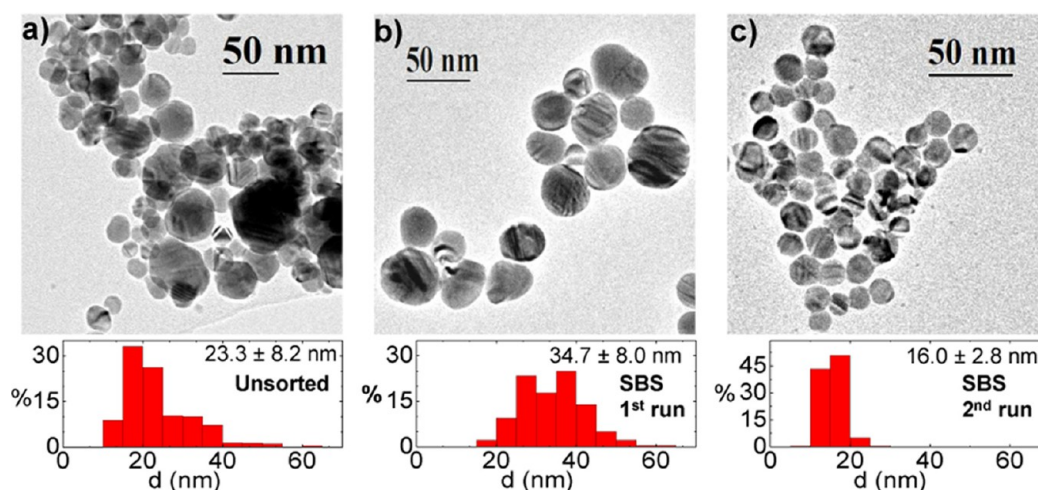
Figure 10. Representative TEM images and size distribution of AgNPs (a) before and (b,c) after selective SBS, at (b) 250 and (c) 550 rcf.

centrifugation time are crucial parameters for reducing the polydispersivity of sorted MNPs. In particular, by increasing the rcf and reducing the centrifugation time, the polydispersivity of the sorted AuNPs increases: by centrifugation either at 750 rcf for 1 h, at 5000 rcf for 30 min, or at 11 000 rcf for 15 min, we obtain, respectively, SD of 22%, 30%, and 45% of the average AuNP size. As shown in Figure 10, our selective SBS is successful also in sorting AgNPs prepared by LASiS in water. As for Figure 10a, the unsorted AgNPs have average dimensions ~23.3 nm with SD ~35%. After the first run of SBS, in the 50−200 rcf range, the AgNPs sediment at the bottom of the cuvette, with average size ~34.7 nm and SD ~23%. AgNPs of reduced size are extracted after the second run of selective SBS in the 250−750 rcf range, see Figure 10b. Indeed, in Figure 10c the extracted AgNPs have average dimension ~16 nm and a SD ~17% (see Table 1). This proves the effectiveness and the universality (i.e., its adaption to different nanomaterials) of selective SBS for NP sorting, while requiring low centrifugal fields, achievable with ordinary benchtop centrifuges, and no gradient preparation and rcf, unlike VG-RZS.

■ DISCUSSION

As summarized in Table 1, MNPs selected in size via VG-RZS in high viscosity pure media have lower SD with respect to selective SBS. In general, size selection in centrifugal fields takes place when a difference in velocity between NPs of different size is generated.[78] Neglecting particle−particle interactions[78] and diffusive effects,[78] the sedimentation velocity (v, m s^{-1}) of a spherical NP in a liquid medium has the following expression:[78]

$$v = c \frac{d^2(\rho_{NP} - \rho_L)}{\eta} g \cdot \text{rcf} \tag{1}$$

where c is a dimensionless parameter depending on the geometrical shape of the nanoparticles, d [m] its diameter, ρ_{NP} and ρ_L [kg m^{-3}] are the NP and liquid medium densities, respectively, η [kg m^{-1} s^{-1}] is the liquid viscosity. The rcf linearly increases with the distance of the object from the center of the rotor according to:[78]

$$\text{rcf} = (r_0 + x) \frac{\omega^2}{g} \tag{2}$$

where r_0 [m] is the radius of the rotor, x [m] the distance of the object from r_0, and ω [rad s^{-1}] the angular velocity. In our VG-RZS experiments, we have different layers (1 mL each)
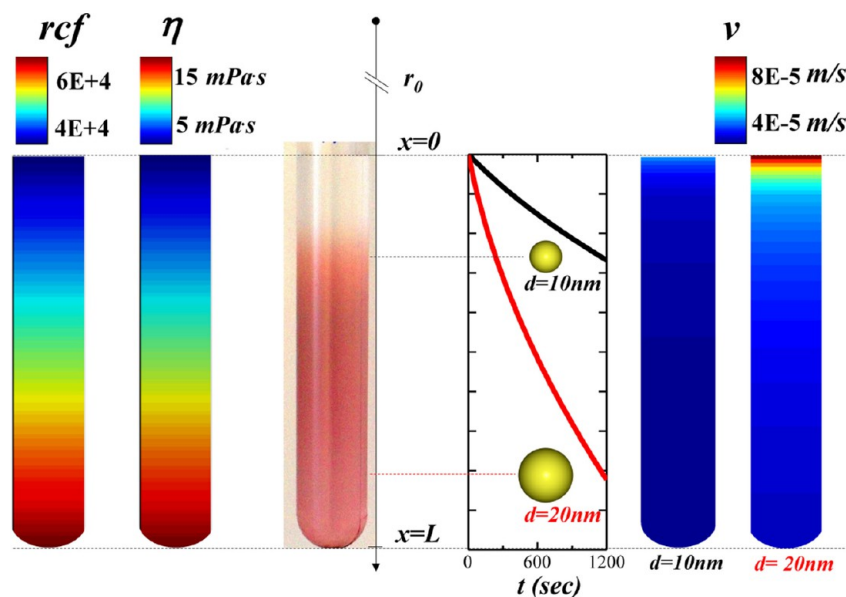
Figure 11. Schematic of selection via VG-RZS in high viscosity media: rcf and η increase along the cuvette from $x = 0$ to $x = L$. The resultant ν of AuNPs drops 10 times from $x = 0$ to $x = L$. Size selection, after 1200 s ultracentrifugation at 20 krpm; 10 nm AuNPs are still in the upper part of the cuvette (black line in the $x(t)$ plot), while 20 nm AuNPs move towards the lower part.

prepared by mixing water (0.9 mPa·s at 25 °C) with ethylene glycol (16.1 mPa·s) with proportions of EG/H_2O varying linearly from 1:0 to 0.2:0.8 from the bottom to the top in 9 successive steps (Figure 8); therefore, η increases up to 18 times[132] for x varying from 0 (top of the cuvette) to $L = 9$ cm (bottom), while ρ_L increases only 10% from $x = 0$ to $x = L$.[132] Thus, as a first approximation, the variation of ρ_L along the cuvette has negligible effect on ν, when compared to the contribution deriving from the variation of η.

As shown in the example of Figure 11, ν of a spherical AuNP moving from the top to the bottom of a cuvette drops ~10 times with x due to the η increase. Moreover, from eq 2, the velocity of a 10 nm AuNP is 4 times smaller than a 20 nm AuNP located at the same x along the cuvette. The velocity of inorganic NPs, such as AuNPs, never reaches 0 along the cuvette because ρ_L is lower than ρ_{NP} for every x. Thus, the ultracentrifugation time plays a fundamental role because, if the ultracentrifugation were to be carried out for long periods, the NPs would all sediment at the bottom. By numerical integration of $x(t) = \nu(x,t) \cdot t$, we calculate[133] that, after 20 min of ultracentrifugation at 20 krpm in the H_2O/EG gradient, 10 nm AuNPs are still located in the upper part of the cuvette ($x = 2.3$ cm), while 20 nm AuNPs move to the lower part ($x = 7.2$ cm, Figure 11), in fair agreement with experiments.

Indeed, the FWHM of the SPR band of AuNPs decreases with the increase of d; see Figure 12a. For a 20 nm AuNP (measured by TEM, see Figure 2), the corresponding FWHM is ~58 nm, while for 9.5 nm, the FWHM is ~76 nm. Figure 12b shows how the FWHM increases with the inverse of the square root of the distance from the top of the cuvette. The gradient formed by high viscosity media has the function of slowing down NPs with increasing size, by progressively decreasing their ν along the cuvette (Figure 11). This also suggests that the intensity of the centrifugal field and the ultracentrifugation time can be adjusted to target sorting of a specific size range on demand.

In selective SBS there are two main differences with respect to VG-RZS: (i) no gradient media are required and (ii) the
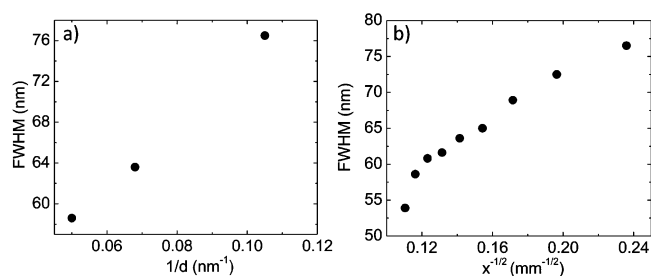
Figure 12. (a) AuNPs SPR band FWHM as a function of the experimental d determined via TEM. (b) AuNPs SPR band FWHM as a function of the inverse of the square root of the distance from the top of the cuvette.

entire cuvette is filled with the NP dispersion, unlike VG-RZS, where NPs are uploaded only at the top of the cuvette. Although the geometry of our problem is complex because we use a 45° fixed angle rotor and Eppendorf cuvettes, we can draw a picture of the mechanism by using a simple model of a spherical particle moving in a liquid medium in a cylindrical cuvette under the force generated by a centrifugal field in a swinging bucket rotor. According to eqs 1 and 2, ν depends on the NP position along the cuvette. Considering NPs located at the mid point ($x = L/2$) of a cylindrical cuvette filled with 1 mL of dispersion, i.e., with a liquid level $L = 1.5$ cm (see Figure 13) and a rotor radius $r_0 = 8.8$ cm, in our experimental conditions, we have that $L/2 < 0.1 r_0$. Consequently, the difference of ν ($\Delta\nu$) between NPs with the same size located at the top ($x = 0$) or at the bottom ($x = L$) is <10%. Therefore, we can assume, as a first approximation:

$$L/2 \approx 0.1 r_0 \rightarrow \text{rcf} \approx r_0 \frac{\omega^2}{g} \qquad (3)$$

We note that, in the selective SBS experiments, we reduced the level of liquid in the cuvette to 1 mL in order to decrease $\Delta\nu$ of same size NPs, located at different x. However, larger volumes of dispersion can be processed by using larger cuvettes, or
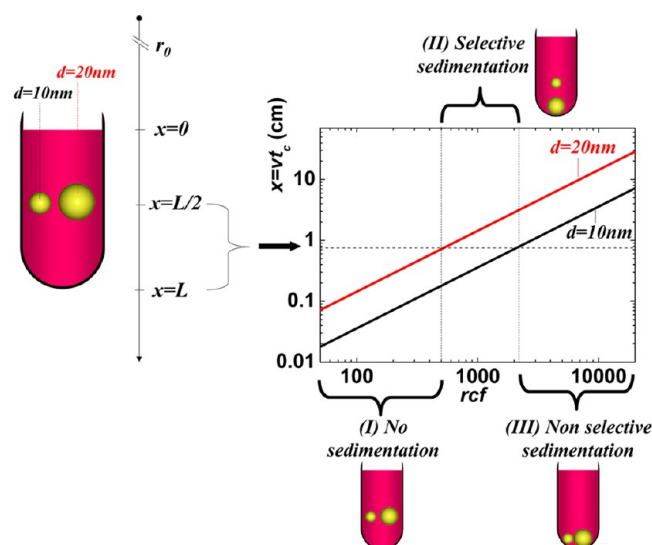
Figure 13. Basic principle of selective SBS: 20 nm AuNPs travel 4 times faster than 10 nm AuNPs located at the same position along the cuvette. After a centrifugation time t_c, we can identify 3 regions in the plot of $x(t_c) = \nu t_c$ versus rcf: in region (I), no sedimentation of AuNPs takes place; in region (II), selective sedimentation of 20 nm AuNPs takes place because $x(d = 20\ \text{nm}, t_c) \geq L/2$ and $x(d = 10\ \text{nm}, t_c) \leq L/2$; in region (III), non-selective sedimentation of AuNPs takes place because $x(d = 20\ \text{nm}, t_c) > L/2$ and $x(d = 10\ \text{nm}, t_c) > L/2$.

rotors with a longer r_0, in order to maintain a low x/r_0 ratio. Under the assumptions of eq 3, ν is also independent of x, and we can express the length traveled by a NP after the centrifugation time t_c as:

$$x(t_c) = c\frac{d^2(\rho_{\text{NP}} - \rho_{\text{L}})}{\eta}g \cdot \text{rcf} \cdot t_c \tag{4}$$

According to eq 4, the ratio of length traveled by 10 and 20 nm AuNPs after t_c is given by the ratio of the square of their diameters:

$$\frac{x(d = 20\ \text{nm},\ t_c)}{x(d = 10\ \text{nm},\ t_c)} = \frac{(d = 20\ \text{nm})^2}{(d = 10\ \text{nm})^2} = 4 \tag{5}$$

The separation of 20 nm AuNPs from 10 nm AuNPs initially located at $x = L/2$ is achieved when $x(d = 20\ \text{nm}, t_c) > L/2$ and $x(d = 10\ \text{nm}, t_c) < L/2$. E.g., for $t_c = 3600$ s, in the plot of $x(t_c) = \nu t_c$ versus rcf (see Figure 13), there are 3 regions corresponding to 3 different ranges of rcf: (I) at low rcf (below 525), no NP selective sedimentation takes place over t_c; (II) at intermediate rcfs (between 525 and 2100), selective sedimentation of 20 nm AuNPs is possible; (III) at high rcf (above 2100), non-selective sedimentation of both 10 and 20 nm AuNPs takes place. Thus, selective sedimentation requires that (a) ν among NPs with the same size located at different x is minimized and (b), for a fixed t_c, the rcf is set to the appropriate range, e.g., 525–2100 for $t_c = 3600$ s in the example of Figure 13. These separation strategies have general validity and are not restricted to the NPs reported in this article. In principle, by tuning the experimental conditions, one could separate NPs of any material.

CONCLUSIONS

We demonstrated the viability of two sorting methodologies for size selection of nanoparticles by centrifugal fields in clean media without the use of chemical additives or other solutes.

Both methods allowed us to prepare size selected metal nanoparticles in the 10–30 nm range, dispersed either in water or in organic solvents. These can be implemented in common benchtop centrifuges, with low intensity centrifugal fields. Rate zonal separation in a viscosity gradient is the most accurate size sorting technique, allowing us to achieve separation of Au metallic nanoparticles ranging from 9.5 nm with standard deviation 11% to 20 nm with standard deviation of 18%. Similar results were also achieved with selective sedimentation-based separation, although with slightly higher standard deviation (from 22 to 30%), but with the advantage that the latter does not require any modification of the initial nanoparticle dispersion.

AUTHOR INFORMATION

Corresponding Author

*(V.A.) E-mail: vincenzo.amendola@unipd.it.

Notes

The authors declare no competing financial interest.

REFERENCES

(1) Stellacci, F. Nanoscale Materials: A New Season. *Nat. Mater.* **2005**, *4*, 113−114.

(2) Pileni, M. Supracrystals of Inorganic Nanocrystals: An Open Challenge for New Physical Properties. *Acc. Chem. Res.* **2008**, *41*, 1799−1809.

(3) Carney, R. P.; Kim, J. Y.; Qian, H.; Jin, R.; Mehenni, H.; Stellacci, F.; Bakr, O. M. Determination of Nanoparticle Size Distribution Together With Density or Molecular Weight by 2D Analytical Ultracentrifugation. *Nat. Commun.* **2011**, *2*, 335.

(4) Cademartiri, L.; Montanari, E.; Calestani, G.; Migliori, A.; Guagliardi, A.; Ozin, G. A. Size-Dependent Extinction Coefficients of PbS Quantum Dots. *J. Am. Chem. Soc.* **2006**, *128*, 10337−10346.

(5) Amendola, V.; Meneghetti, M. Size Evaluation of Gold Nanoparticles by UV−vis Spectroscopy. *J. Phys. Chem. C* **2009**, *113*, 4277−4285.

(6) Amendola, V.; Meneghetti, M. Exploring How to Increase the Brightness of Surface-Enhanced Raman Spectroscopy Nanolabels: The Effect of the Raman-Active Molecules and of the Label Size. *Adv. Funct. Mater.* **2012**, *22*, 353−360.

(7) Lagos, N.; Sigalas, M. M.; Lidorikis, E. Theory of Plasmonic Near-Field Enhanced Absorption in Solar Cells. *Appl. Phys. Lett.* **2011**, *99*, 063304.

(8) Boisselier, E.; Astruc, D. Gold Nanoparticles in Nanomedicine: Preparations, Imaging, Diagnostics, Therapies and Toxicity. *Chem. Soc. Rev.* **2009**, *38*, 1759−1782.

(9) Niemeyer, C. M. Nanoparticles, Proteins, and Nucleic Acids: Biotechnology Meets Materials Science. *Angew. Chem., Int. Ed.* **2001**, *40*, 4128−4158.

(10) Jain, P. K.; Huang, X.; El-Sayed, I. H.; El-Sayed, M. A. Noble Metals on the Nanoscale: Optical and Photothermal Properties and Some Applications in Imaging, Sensing, Biology, and Medicine. *Acc. Chem. Res.* **2008**, *41*, 1578−1586.

(11) Kreibig, U.; Vollmer, M. *Optical Properties of Metal Clusters*; Springer: Berlin, Germany, 1995.

(12) Berciaud, S.; Cognet, L.; Tamarat, P.; Lounis, B. Observation of Intrinsic Size Effects in the Optical Response of Individual Gold Nanoparticles. *Nano Lett.* **2005**, *5*, 515−518.

(13) Kreibig, U.; Genzel, U. Optical Absorption of Small Metallic Particles. *Surf. Sci.* **1985**, *156*, 678.

(14) Boyer, D.; Tamarat, P.; Maali, A.; Lounis, B.; Orrit, M. Photothermal Imaging of Nanometer-Sized Metal Particles Among Scatterers. *Science* **2002**, *297*, 1160−1163.

(15) Mallidi, S.; Larson, T.; Tam, J.; Joshi, P. P.; Karpiouk, A.; Sokolov, K.; Emelianov, S. Multiwavelength Photoacoustic Imaging and Plasmon Resonance Coupling of Gold Nanoparticles for Selective Detection of Cancer. *Nano Lett.* **2009**, *9*, 2825−2831.

(16) Shao, D. B.; Chen, S. C. Surface-Plasmon-Assisted Nanoscale Photolithography by Polarized Light. *Appl. Phys. Lett.* **2005**, *86*, 253107.

(17) Csaki, A.; Garwe, F.; Steinbrück, A.; Maubach, G.; Festag, G.; Weise, A.; Riemann, I.; König, K.; Fritzsche, W. A Parallel Approach for Subwavelength Molecular Surgery Using Gene-Specific Positioned Metal Nanoparticles as Laser Light Antennas. *Nano Lett.* **2007**, *7*, 247−253.

(18) Meulenkamp, E. A. Size Dependence of the Dissolution of ZnO Nanoparticles. *J. Phys. Chem. B* **1998**, *102*, 7764−7769.

(19) Daniel, M.-C.; Astruc, D. Gold Nanoparticles: Assembly, Supramolecular Chemistry, Quantum-Size-Related Properties, and Applications Toward Biology, Catalysis, and Nanotechnology. *Chem. Rev.* **2004**, *104*, 293−346.

(20) Zhou, X.; Xu, W.; Liu, G.; Panda, D.; Chen, P. Size-Dependent Catalytic Activity and Dynamics of Gold Nanoparticles at the Single-Molecule Level. *J. Am. Chem. Soc.* **2010**, *132*, 138−146.

(21) Sau, T. K.; Pal, A.; Pal, T. Size Regime Dependent Catalysis by Gold Nanoparticles for the Reduction of Eosin. *J. Phys. Chem. B* **2001**, *105*, 9266−9272.

(22) Brey, W. S.; Krieger, K. A. The Surface Area and Catalytic Activity of Aluminum Oxide. *J. Am. Chem. Soc.* **1949**, *71*, 3637−3641.

(23) Roca, A. G.; Costo, R.; Rebolledo, A. F.; Veintemillas-Verdaguer, S.; Tartaj, P.; Gonzalez-Carreno, T.; Morales, M. P.; Serna, C. J. Progress in the Preparation of Magnetic Nanoparticles for Applications in Biomedicine. *J. Phys. D: Appl. Phys.* **2009**, *42*, 224002−224012.

(24) Seo, W. S.; Jo, H. H.; Lee, K.; Kim, B.; Oh, S. J.; Park, J. T. Size-Dependent Magnetic Properties of Colloidal Mn_3O_4 and MnO Nanoparticles. *Angew. Chem., Int. Ed.* **2004**, *43*, 1115−1117.

(25) Amendola, V.; Riello, P.; Polizzi, S.; Fiameni, S.; Innocenti, C.; Sangregorio, C.; Meneghetti, M. Magnetic Iron Oxide Nanoparticles with Tunable Size and Free Surface Obtained via a "Green" Approach Based on Laser Irradiation in Water. *J. Mater. Chem.* **2011**, *21*, 18665−18673.

(26) Etheridge, M. L.; Campbell, S. A.; Erdman, A. G.; Haynes, C. L.; Wolf, S. M.; McCullough, J. The Big Picture on Nanomedicine: the State of Investigational and Approved Nanomedicine Products. *Nanomed. Nanotechnol. Biol. Med.* **2013**, *9*, 1−14.

(27) Akhter, S.; Ahmad, M. Z.; Ahmad, F. J.; Storm, G.; Kok, R. J. Gold Nanoparticles in Theranostic Oncology: Current State-of-the-Art. *Expert Opin. Drug. Delivery* **2012**, *9:10*, 1225−1243.

(28) Chien, C.-C.; Cheng, C.-C.; Chen, H. H.; Hwu, Y.; Chu, Y. S.; Petibois, C.; Chen, A.; Ching, Y.-T.; Margaritondo, G. X-Ray Microscopy and Tomography Detect the Accumulation of Bare and PEG-coated Gold Nanoparticles in Normal and Tumor Mouse Tissues. *Anal. Bioanal. Chem.* **2012**, *404:5*, 1287−1296.

(29) Kim, D.; Park, S.; Lee, J. H.; Jeong, Y. Y.; Jon, S. Antibiofouling Polymer-Coated Gold Nanoparticles as a Contrast Agent for in Vivo X-Ray Computed Tomography Imaging. *J. Am. Chem. Soc.* **2007**, *129*, 7661−7665.

(30) Kupffer, K. V. mit Portr-t. *Mit Porträt Archiv fr Mikroskopische Anatomie* **1903**, *62*, 669−718.

(31) De Jong, W. H.; Hagens, W. I.; Krystek, P.; Burger, M. C.; Sips, A. J. A. M.; Geertsma, R. E. Particle Size-Dependent Organ Distribution of Gold Nanoparticles after Intravenous Administration. *Biomaterials* **2008**, *29*, 1912−1919.

(32) Verma, A.; Uzun, O.; Hu, Y.; Hu, Y.; Han, H. S.; Watson, N.; Chen, S.; Irvine, D. J.; Stellacci, F. Surface-Structure-Regulated Cell-Membrane Penetration by Monolayer-Protected Nanoparticles. *Nat. Mater.* **2008**, *7*, 588−595.

(33) Chithrani, B. D.; Chan, W. C. W. Elucidating the Mechanism of Cellular Uptake and Removal of Protein-Coated Gold Nanoparticles of Different Sizes and Shapes. *Nano Lett.* **2007**, *7*, 1542−1550.

(34) Chithrani, B. D.; Ghazani, A. A.; Chan, W. C.W. Determining the Size and Shape Dependence of Gold Nanoparticle Uptake into Mammalian Cells. *Nano Lett.* **2006**, *6*, 662−668.

(35) Rothman, J. E. Mechanisms of Intracellular Protein Transport. *Nature* **1994**, *372*, 55−63.

(36) Murphy, C. J.; Gole, A. M.; Stone, J. W.; Sisco, P. N.; Alkilany, A. M.; Goldsmith, E. C.; Baxter, S. C. Gold Nanoparticles in Biology: Beyond Toxicity to Cellular Imaging. *Acc. Chem. Res.* **2008**, *41*, 1721−1730.

(37) Atwater, H. A.; Polman, A. Plasmonics for Improved Photovoltaic Devices. *Nat. Mater.* **2010**, *9*, 205−213.

(38) Echtermeyer, T. J.; Britnell, L.; Jasnos, P. K.; Lombardo, A.; Gorbachev, R. V.; Grigorenko, A. N.; Geim, A. K.; Ferrari, A. C.; Novoselov, K. S. Strong Plasmonic Enhancement of Photovoltage in Graphene. *Nat. Commun.* **2011**, *2*, 458.

(39) Andrew, P.; Barnes, W. L. Energy Transfer Across a Metal Film Mediated by Surface Plasmon Polaritons. *Science* **2004**, *306*, 1002−1005.

(40) Quinten, M.; Leitner, A.; Krenn, J. R.; Aussenegg, F. R. Electromagnetic Energy Transport via Linear Chains of Silver Nanoparticles. *Opt. Lett.* **1998**, *23*, 1331−133.

(41) Fleischmann, M.; Hendra, P. J.; McQuillan, A. J. Raman Spectra of Pyridine Adsorbed at a Silver Electrode. *Chem. Phys. Lett.* **1974**, *26*, 163.

(42) Schedin, F.; Lidorikis, E.; Lombardo, A.; Kravets, V. G.; Geim, A. K.; Grigorenko, A. N.; Novoselov, K. S.; Ferrari, A. C. Surface Enhanced Raman Spectroscopy of Graphene. *ACS Nano* **2010**, *4*, 5617−5626.

(43) Fazio, B.; D'Andrea, C.; Bonaccorso, F.; Irrera, A.; Calogero, G.; Vasi, C.; Gucciardi, P. G.; Allegrini, M.; Toma, A.; Chiappe, D.; Martella, C.; Buatier de Mongeot, F. Re-Radiation Enhancement in Polarized Surface-Enhanced Resonant Raman Scattering of Randomly Oriented Molecules on Self-Organized Gold Nanowires. *ACS Nano* **2011**, *5*, 5945−5956.

(44) Bello, J. M.; Narayanan, V. A.; Stokes, D. L.; Vo-Dinh, T. Fiber-Optic Remote Sensor for in Situ Surface-Enhanced Raman Scattering Analysis. *Anal. Chem.* **1990**, *62*, 2437−2441.

(45) Foti, A.; D'Andrea, C.; Bonaccorso, F.; Lanza, M.; Calogero, G.; Messina, E.; Maragó, O. M.; Fazio, B.; Gucciardi, P. G. A Shape-Engineered Surface-Enhanced Raman Scattering Optical Fiber Sensor Working from the Visible to the Near-Infrared. *Plasmonics* **2013**, *8*, 13−23.

(46) Mühlschlegel, P.; Eisler, H. J.; Martin, O. J. F.; Hecht, B.; Pohl, D. W. Resonant Optical Antennas. *Science* **2005**, *308*, 1607−1609.

(47) Amendola, V.; Meneghetti, M. Laser Ablation Synthesis in Solution and Size Manipulation of Noble Metal Nanoparticles. *Phys. Chem. Chem. Phys.* **2009**, *11*, 3805−3821.

(48) Reineck, P.; Lee, G. P.; Brick, D.; Karg, M.; Mulvaney, P.; Bach, U. A Solid-State Plasmonic Solar Cell via Metal Nanoparticle Self-Assembly. *Adv. Mater.* **2012**, *24*, 4750−4755.

(49) Bai, L.; Ma, X.; Liu, J.; Sun, X.; Zhao, D.; Evans, D. G. Rapid Separation and Purification of Nanoparticles in Organic Density Gradients. *J. Am. Chem. Soc.* **2010**, *132*, 2333−2337.

(50) Zhang, C.; Luo, L.; Luo, J.; Evans, D. G.; Sun, X. A Process-Analysis Microsystem Based on Density Gradient Centrifugation and Its Application in the Study of the Galvanic Replacement Mechanism of Ag Nanoplates with $HAuCl_4$. *Chem. Commun.* **2012**, *48*, 7241−7243.

(51) Akbulut, O.; Mace, C. R.; Martinez, R. V.; Kumar, A. A.; Nie, Z.; Patton, M. R.; Whitesides, G. M. Separation of Nanoparticles in Aqueous Multiphase Systems through Centrifugation. *Nano Lett.* **2012**, *12*, 4060−4064.

(52) Chen, G.; Wang, Y.; Tan, L. H.; Yang, M.; Tan, L. S.; Chen, Y.; Chen, H. High-Purity Separation of Gold Nanoparticle Dimers and Trimers. *J. Am. Chem. Soc.* **2009**, *131*, 4218−4219.

(53) Zook, J. M.; Rastogi, V.; MacCuspie, R. I.; Keene, A. M.; Fagan, J. Measuring Agglomerate Size Distribution and Dependence of Localized Surface Plasmon Resonance Absorbance on Gold Nano-particle Agglomerate Size Using Analytical Ultracentrifugation. *ACS Nano* **2011**, *5*, 8070−8079.

(54) Qiu, P.; Mao, C. Viscosity Gradient as a Novel Mechanism for the Centrifugation-Based Separation of Nanoparticles. *Adv. Mater.* **2011**, *23*, 4880−4885.

(55) Tyler, T. P.; Henry, A. I.; Van Duyne, R. P.; Hersam, M. C. Improved Monodispersity of Plasmonic Nanoantennas via Centrifugal Processing. *J. Phys. Chem. Lett.* **2011**, *2*, 218−222.

(56) Li, S.; Chang, Z.; Liu, J.; Bai, L.; Luo, L.; Sun, X. Separation of Gold Nanorods Using Density Gradient Ultracentrifugation. *Nano Res.* **2011**, *4*, 723−728.

(57) Sun, S.; Murray, C. B.; Weller, D.; Folks, L.; Moser, A. Monodisperse FePt Nanoparticles and Ferromagnetic FePt Nano-crystal Superlattices. *Science* **2000**, *287*, 1989−1992.

(58) Park, J.; Kang, E.; Son, S. U.; Park, H. M.; Lee, M. K.; Kim, J.; Kim, K. W.; Noh, H.-J.; Park, J.-H.; Bae, C. J.; Park, J.-G.; Hyeon, T. Monodisperse Nanoparticles of Ni and NiO: Synthesis, Character-ization, Self-Assembled Superlattices, and Catalytic Applications in the Suzuki Coupling Reaction. *Adv. Mater.* **2005**, *17*, 429−434.

(59) Yi, D. K.; Selvan, S. T.; Lee, S. S.; Papaefthymiou, G. C.; Kundaliya, D.; Ying, J. Y. Silica-Coated Nanocomposites of Magnetic Nanoparticles and Quantum Dots. *J. Am. Chem. Soc.* **2005**, *127*, 4990−4991.

(60) Sun, Y.; Xia, Y. Shape-Controlled Synthesis of Gold and Silver Nanoparticles. *Science* **2002**, *298*, 2176−2179.

(61) Hu, J.; Li, L.; Yang, W.; Manna, L.; Wang, L.; Alivisatos, A. P. Linearly Polarized Emission from Colloidal Semiconductor Quantum Rods. *Science* **2001**, *292*, 2060−2063.

(62) Kimling, J.; Maier, M.; Okenve, B.; Kotaidis, V.; Ballot, M.; Plech, A. Turkevich Method for Gold Nanoparticle Synthesis Revisited. *J. Phys. Chem. B* **2006**, *110*, 15700−15707.

(63) Sun, X.; Tabakman, S. M.; Seo, W. S.; Zhang, L.; Zhang, G.; Sherlock, S.; Bai, L.; Dai, H. High-Purity Separation of Gold Nanoparticle Dimers and Trimers. *Angew. Chem., Int. Ed.* **2009**, *48*, 939−942.

(64) Khan, U.; O'Neill, A.; Porwal, H.; May, P.; Nawaz, N.; Coleman, J. N. Size Selection of Dispersed, Exfoliated Graphene Flakes by Controlled Centrifugation. *Carbon* **2012**, *50*, 470−475.

(65) Sweeney, S. F.; Woehrle, G. H.; Hutchison, J. E. Rapid Purification and Size Separation of Gold Nanoparticles via Diafiltration. *J. Am. Chem. Soc.* **2006**, *128*, 3190−3197.

(66) Hanauer, M.; Pierrat, S.; Zins, I.; Lotz, A.; Sonnichsen, C. Separation of Nanoparticles by Gel Electrophoresis According to Size and Shape. *Nano Lett.* **2007**, *7*, 2881−2885.

(67) O'Neill, A.; Khan, U.; Coleman, J. N. Preparation of High Concentration Dispersions of Exfoliated MoS$_2$ with Increased Flake Size. *Chem. Mater.* **2012**, *24*, 2414−2421.

(68) Novak, J. P.; Nickerson, C.; Franzen, S.; Feldheim, D. L. Purification of Molecularly Bridged Metal Nanoparticle Arrays by Centrifugation and Size Exclusion Chromatography. *Anal. Chem.* **2001**, *73*, 5758−5761.

(69) Falabella, J. B.; Cho, T. J.; Ripple, D. C.; Hackley, V. A. Characterization of Gold Nanoparticles Modified with Single-Stranded DNA Using Analytical Ultracentrifugation and Dynamic Light Scattering. *Langmuir* **2010**, *26*, 12740−12747.

(70) Caragheorgheopol, A.; Chechik, V. Mechanistic Aspects of Ligand Exchange in Au Nanoparticles. *Phys. Chem. Chem. Phys.* **2008**, *10*, 5029−5041.

(71) Wang, X.; Li, G.; Chen, T.; Yang, M.; Zhang, Z.; Wu, T.; Chen, H. Polymer-Encapsulated Gold-Nanoparticle Dimers: Facile Prepara-tion and Catalytical Application in Guided Growth of Dimeric ZnO-Nanowires. *Nano Lett.* **2008**, *8*, 2643−2647.

(72) Lee, J. S.; Stoeva, S. I.; Mirkin, C. A. DNA-Induced Size-Selective Separation of Mixtures of Gold Nanoaparticles. *J. Am. Chem. Soc.* **2006**, *128*, 8899−8903.

(73) Mafune, F.; Kohno, J.; Takeda, Y.; Kondow, T. Full Physical Preparation of Size-Selected Gold Nanoparticles in Solution: Laser Ablation and Laser-Induced Size Control. *J. Phys. Chem. B* **2002**, *106*, 7575−7577.

(74) Werner, D.; Ueki, T.; Hashimoto, T. Methodological Improve-ment in Pulsed Laser-Induced Size Reduction of Aqueous Colloidal Gold Nanoparticles by Applying High Pressure. *J. Phys. Chem. C* **2012**, *116*, 5482−5491.

(75) Svedberg, T.; Pedersen, K. O. *The Ultracentrifuge*; Oxford University Press: London, U.K., 1940.

(76) Pickels, E. G. Sedimentation in the Angle Centrifuge. *Gen. Physiol.* **1943**, *26*, 341−359.

(77) Behrens, M. Hoppe-Seyler's Über die Verteilung: der Lipase und Arginase Zwischen Zellkern und Protoplasma der Leber. *Z. Physiol. Chem.* **1939**, *258*, 27−32.

(78) Williams, J. W.; Van Holde, K. E.; Baldwin, R. L.; Fujita, H. The Theory of Sedimentation Analysis. *Chem. Rev.* **1958**, *58*, 715−806.

(79) Ifft, J. B.; Vinograd, J. The Buoyant Behavior of Bovine Serum Mercaptalbumin in Salt Solutions at Equilibrium in the Ultra-centrifuge. II. Net Hydration, Ion Binding, and Solvated Molecular Weight in Various Salt Solutions. *J. Phys. Chem.* **1966**, *70*, 2814−2822.

(80) Bonaccorso, F.; Hasan, T.; Tan, P. H.; Sciascia, C.; Privitera, G.; Di Marco, G.; Gucciardi, P. G.; Ferrari, A. C. Density Gradient Ultracentrifugation of Nanotubes: Interplay of Bundling and Surfactant Encapsulation. *J. Phys. Chem. C* **2010**, *114*, 17267−12285.

(81) Brakke, M. K. Zonal Separations by Density-Gradient Centrifugation. *Arch. Biochem.* **1953**, *45*, 275−290.

(82) Patel, D.; Rickwood, D. Optimization of Condition for Specific Binding of Antibody-Coated Beads to Cells. *J. Immunol. Methods* **1995**, *184*, 71−80.

(83) Bildirici, L.; Rickwood, D. Fractionation of Differentiating Cells Using Density Perturbation. *J. Immunol. Methods* **2000**, *240*, 93−99.

(84) Hayashi, Y.; Bird, F. T. The Use of Sucrose Gradients in the Isolation of Cytoplasmic-Polyhedrosis Virus Particles. *J. Invertebr. Pathol.* **1968**, *11*, 40−44.

(85) Rosenbloom, J.; Schumaker, V. N. Analytical Ultracentrifugation of T4r Bacteriophage DNA in Preformed Sucrose Density Gradient. *Biochemistry* **1963**, *2*, 1206.

(86) Arnold, M. S.; Stupp, S. I.; Hersam, M. C. Enrichment of Single-Walled Carbon Nanotubes by Diameter in Density Gradients. *Nano Lett.* **2005**, *5*, 713−718.

(87) Arnold, M. S.; Green, A. A.; Hulvat, J. F.; Stupp, S. I.; Hersam, M. C. Sorting Carbon Nanotubes by Electronic Structure Using Density Differentiation. *Nat. Nanotechnol.* **2006**, *1*, 60−65.

(88) Green, A. A.; Duch, M. C.; Hersam, M. C. Isolation of Single-Walled Carbon Nanotube Enantiomers by Density Differentiation. *Nano Res.* **2009**, *2*, 69−77.

(89) Ghosh, S.; Bachilo, S. M.; Weisman, R. B. Advanced Sorting of Single-Walled Carbon Nanotubes by Nonlinear Density-Gradient Ultracentrifugation. *Nat. Nanotechnol.* **2010**, *5*, 443−450.

(90) Green, A. A.; Hersam, M. C. Solution Phase Production of Graphene with Controlled Thickness via Density Differentiation. *Nano Lett.* **2009**, *9*, 4031−4036.

(91) Fagan, J. A.; Becker, M. L.; Chun, J.; Nie, P.; Bauer, B. J.; Simpson, J. R.; Hight-Walker, A.; Hobbie, E. K. Centrifugal Length Separation of Carbon Nanotubes. *Langmuir* **2008**, *24*, 13880−13889.

(92) Sun, X.; Luo, D.; Liu, J.; Evans, D. G. Monodisperse Chemically Modified Graphene Obtained by Density Gradient Ultracentrifugal Rate Separation. *ACS Nano* **2010**, *4*, 3381−3389.

(93) Mastronardi, M. L.; Hennrich, F.; Henderson, E. J.; Maier-Flaig, F.; Blum, C.; Reichenbach, J.; Lemmer, U.; Keubel, C.; Wang, D.; Kappes, M. M.; Ozin, G. A. Preparation of Monodisperse Silicon Nanocrystals Using Density Gradient Ultracentrifugation. *J. Am. Chem. Soc.* **2011**, *133*, 11928−11931.

(94) Zhitomirsky, D.; Kramer, I. J.; Labelle, A. J.; Fischer, A.; Debnath, R.; Pan, J.; Bakr, O. M.; Sargent, E. H. Colloidal Quantum

13228

dx.doi.org/10.1021/jp400599g | *J. Phys. Chem. C* 2013, 117, 13217−13229

Dot Photovoltaics: The Effect of Polydispersity. *Nano Lett.* **2012**, *12*, 1007−1012.

(95) Whitman, J. L.; Clardy, L. Densities and Refractive Indices of Bromoform−Benzene Mixtures. *J. Am. Chem. Soc.* **1936**, *58*, 237−239.

(96) Sollas, W. L. A Method of Determining Specific Gravity. *Nature* **1891**, *43*, 404−405.

(97) Boswell, P. G. H. The Application of Petrological and Quantitative Methods to Stratigraphy. *Geol. Mag.* **1916**, *3*, 105−111.

(98) Munsterman, D.; Kersholt, S. Sodium Polytungstate, a New Non-Toxic Alternative to Bromoform in Heavy Liquid Separation. *Rev. Palaeobot. Palynol.* **1996**, *91*, 417−422.

(99) MSDS: Sodium Polytungstate. http://www.geoliquids.com/geo_pdfs/msds_sp.pdf.

(100) Kittel, C. *Introduction to Solid State Physics*, 8th ed.; Wiley: New York, 2004.

(101) Wang, J. C. The Degree of Unwinding of the DNA Helix by Ethidium. *J. Mol. Biol.* **1974**, *89*, 783−801.

(102) Brakke, M. K. Density Gradient Centrifugation: A New Separation Technique. *J. Am. Chem. Soc.* **1951**, *73*, 1847−1848.

(103) Coombs, D. H.; Watts, N. R. M. Generating Sucrose Gradients in Three Minutes by Tilted Tube Rotation. *Anal. Biochem.* **1985**, *148*, 254−259.

(104) Kaminsky, M. Ion−Solvent Interaction and the Viscosity of Strong-Electrolyte Solutions. *Discuss. Faraday Soc.* **1957**, *24*, 171−179.

(105) Chenlo, F.; Moreira, R.; Pereira, G.; Ampudia, A. Viscosities of Aqueous Solutions of Sucrose and Sodium Chloride of Interest in Osmotic Dehydration Processes. *J. Food Eng.* **2002**, *54*, 347−352.

(106) Zhang, J.; Kang, D. E.; Xia, W.; Okochi, M.; Mori, H.; Selkoe, D. J.; Koo, E. H. Subcellular Distribution and Turnover of Presenilins in Transfected Cells. *J. Biol. Chem.* **1998**, *273*, 12436−12442.

(107) Collins, K.; Washabaugh, M. The Hoffmeister Effect and the Behaviour of Water at Interfaces. *Q. Rev. Biophys.* **1985**, *18*, 323−422.

(108) Cacace, M. G.; Landau, E. M.; Ramsden, J. J. The Hofmeister Series: Salt and Solvent Effects on Interfacial Phenomena. *Q. Rev. Biophys.* **1997**, *30*, 241−277.

(109) Israelachvili, J. N. *Intermolecular and Surface Forces*, 3rd ed.; Academic Press: New York, 2011.

(110) Gearheart, L. A.; Ploehn, H. J.; Murphy, C. J. Oligonucleotide Adsorption to Gold Nanoparticles: A Surface-Enhanced Raman Spectroscopy Study of Intrinsically Bent DNA. *J. Phys. Chem. B* **2001**, *105*, 12609−12615.

(111) Zhou, J.; Ralston, J.; Sedev, R.; Beattie, D. A. Functionalized Gold Nanoparticles: Synthesis, Structure and Colloid Stability. *J. Colloid Interface Sci.* **2009**, *331*, 251−262.

(112) Kim, T.; Lee, K.; Gong, M.-S.; Joo, S.-W. Control of Gold Nanoparticle Aggregates by Manipulation of Interparticle Interaction. *Langmuir* **2005**, *21*, 9524−9528.

(113) Gellert, G. Sensitivity and Significance of Luminescent Bacteria in Chronic Toxicity Testing Based on Growth and Bioluminescence. *Ecotoxicol. Environ. Saf.* **2000**, *45*, 87−91.

(114) Shin, H.-S.; Yang, H. J.; Kim, S. B.; Lee, M. S. Mechanism of Growth of Colloidal Silver Nanoparticles Stabilized by Polyvinyl Pyrrolidone in γ-Irradiated Silver Nitrate Solution. *J. Colloid Interface Sci.* **2004**, *274*, 89−94.

(115) Vincent, B.; Young, C. A.; Tadros, T. F. Equilibrium Aspects of Heteroflocculation in Mixed Sterically-Stabilised Dispersions. *Faraday Discuss. Chem. Soc.* **1978**, *65*, 296−305.

(116) Shah, H.; Hartman, S. P.; Weinhouse, S. Formation of Carbonyl Chloride in Carbon Tetrachloride Metabolism by Rat Liver in Vitro. *Cancer Res.* **1979**, *39*, 3942−3947.

(117) Compagnini, G.; Scalisi, A. A.; Puglisi, O. Ablation of Noble Metals in Liquids: a Method to Obtain Nanoparticles in a Thin Polymeric Film. *Phys. Chem. Chem. Phys.* **2002**, *4*, 2787−2791.

(118) Crochet, J.; Clemens, M.; Hertel, T. Quantum Yield Heterogeneities of Aqueous Single-Wall Carbon Nanotube Suspensions. *J. Am. Chem. Soc.* **2007**, *129*, 8058−8059.

(119) Mie, G. Beiträge zur Optik Trüber Medien, Speziell Kolloidaler Metallösungen. *Ann. Phys.* **1908**, *3*, 377−445.

(120) Johnson, P. B.; Christy, R. W. Optical Constants of the Noble Metals. *Phys. Rev. B* **1972**, *6*, 4370−4379.

(121) Halperin, W. P. Quantum Size Effects in Metal Particles. *Rev. Mod. Phys.* **1986**, *58*, 533−606.

(122) Kawabata, A.; Kubo, R. Electronic Properties of Fine Metallic Particles. II. Plasma Resonance Absorption. *J. Phys. Soc. Jpn.* **1966**, *21*, 1765−1772.

(123) Link, S.; El-Sayed, M. A. Size and Temperature Dependence of the Plasmon Absorption of Colloidal Gold Nanoparticles. *J. Phys. Chem. B* **1999**, *103*, 4212−4217.

(124) Arnold, G. W. Near-Surface Nucleation and Crystallization of an Ion-Implanted Lithia-Alumina-Silica Glass. *J. Appl. Phys.* **1975**, *46*, 4466.

(125) Amendola, V.; Bakr, O. M.; Stellacci, F. A Study of the Surface Plasmon Resonance of Silver Nanoparticles by the Discrete Dipole Approximation Method: Effect of Shape, Size, Structure, and Assembly. *Plasmonics* **2010**, *5*, 85−97.

(126) Bohren, C. F.; Huffman, D. R. *Absorption and Scattering of Light by Small Particles*; J. Wiley Sons: New York, 1983.

(127) Product Specification Sheet. http://www.sciencelab.com/msds.php?msdsId=9926618.

(128) Cheng, N. S. Formula for Viscosity of Glycerol−Water Mixture. *Ind. Eng. Chem. Res.* **2008**, *47*, 3285−3288.

(129) Messina, E.; Cavallaro, E.; Cacciola, A.; Iati, M. A.; Gucciardi, P. G.; Borghese, F.; Denti, P.; Saija, R.; Compagnini, G.; Meneghetti, M.; Amendola, V.; Maragò, O. M. Plasmon-Enhanced Optical Trapping of Gold Nanoaggregates with Selected Optical Properties. *ACS Nano* **2011**, *5*, 905−913.

(130) Bonaccorso, F.; Sun, Z.; Hasan, T.; Ferrari, A. C. Graphene Photonics and Optoelectronics. *Nat. Photon.* **2010**, *4*, 611−622.

(131) Maragò, O. M.; Bonaccorso, F.; Saija, R.; Privitera, G.; Gucciardi, P. G.; Iatì, M. A.; Calogero, G.; Jones, P. H.; Borghese, F.; Denti, P. Brownian Motion of Graphene. *ACS Nano* **2010**, *4*, 7515−7523.

(132) Tsierkezos, N. G.; Molinou, I. E. Thermodynamic Properties of Water + Ethylene Glycol at 283.15, 293.15, 303.15, and 313.15 K. *J. Chem. Eng. Data* **1998**, *43*, 989−993.

(133) The code used for the evaluation of settling velocity and trajectories can be downloaded from http://www.chimica.unipd.it/vincenzo.amendola/pubblica/sedtrj.zip.